New Journal of Physics
The open access journal for physics

Surface- and point-defect-related Raman scattering in wurtzite semiconductors excited above the band gap

C Kranert[1], R Schmidt-Grund and M Grundmann
Universität Leipzig, Institut für Experimentelle Physik II, Abteilung Halbleiterphysik, Linnéstraße 5, D-04103 Leipzig, Germany
E-mail: christian.kranert@uni-leipzig.de

New Journal of Physics **15** (2013) 113048 (22pp)
Received 3 September 2013
Published 26 November 2013
Online at http://www.njp.org/
doi:10.1088/1367-2630/15/11/113048

Abstract. We present a model for exciton-mediated first-order Raman scattering by longitudinal optical phonons in the presence of surfaces and point defects. It is consistent with the experimental data for all wurtzite structure materials investigated and reviewed here (GaN, InN, ZnO and CdS) and also explains not yet understood observations in the literature. We distinguish between the involvement of elastic scattering by the surface and by point defects in the scattering process. Surface scattering causes the dependence of the line position on the crystal orientation of the excited surface in pure crystals. Point defect scattering is independent of the crystal orientation and appears as an additional contribution in defect-rich crystals. We postulate the polarization properties of these distinct processes which are in good agreement with the experiments and allow us to identify and separate the contributions of these two effects from the polarized spectra.

[1] Author to whom any correspondence should be addressed.

Contents

1. Introduction

Raman scattering is an experimental optical technique that is widely applied for the non-destructive investigation of structural properties like strain, disorder and defects. Defects particularly play an important role for Raman spectra excited above the band gap. In the case of polar crystals such as wurtzites, such spectra primarily show a series of lines from multiple scattering by longitudinal optical (LO) phonons. The dominating physical process causing the observation of the first-order LO peak (1LO) is substantially different from the sole inelastic exciton–phonon scattering causing the higher order peaks, because it requires an additional scattering step breaking the momentum conservation, which leads to an experimentally observed redshift of the 1LO line in the order of several cm^{-1} relative to the respective Γ-point mode. This step can be provided by elastic scattering by defects (cf figure 1). Based on this picture, models were developed to describe the resonance profile of cubic semiconductors for energies around the band gap and also well above it [1–3] by considering an elastic scattering process. Commonly, such elastic scattering has been assumed to be induced by impurities in the samples. Contrary to the isotropic materials studied in these publications, in uniaxial wurtzites the energy of the involved phonons, and thus the spectral position of the 1LO peak, is linked to the direction of the phonon wave vector relative to the crystal axis. The phonon wave vector in turn is determined by the elastic scattering step. Thus, the investigation of the spectral position of the 1LO line in wurtzites, when excited above the band gap, allows us to investigate the properties of this defect-induced elastic scattering.

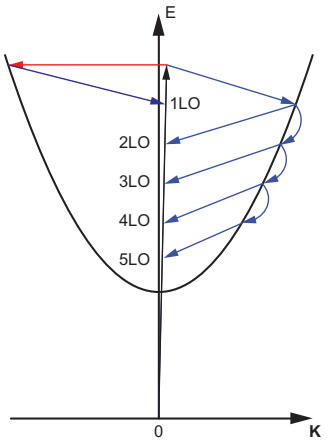

Figure 1. Cascade model for inelastic scattering by phonons only (right hand side) and the extended cascade model which additionally includes an elastic scattering process leading to 1LO emission (left hand side). **K** is the exciton centre-of-mass wave vector, the parabola depicts the dispersion of the discrete exciton states. Blue arrows depict inelastic exciton–phonon scattering, the red (horizontal) arrow depicts elastic scattering of the exciton.

The state of the literature on this topic differs between indium nitride (InN) on the one hand, which is always excited above its small band gap, and wide band gap materials like zinc oxide (ZnO) and gallium nitride (GaN) on the other hand, for which in most publications an excitation below the band gap was chosen. However, for the latter ultraviolet (UV) Raman measurements are also available [4–8] allowing for a comparison between both types of excitation. In the case of InN, the lack of Raman spectra excited below the band gap, accompanied by the fact that samples with sufficiently low charge carrier densities are hard to produce, resulted in a controversy on the actual energy of the two zone centre LO phonons [9–11], because only phonons with large wave vectors are observed. For ZnO and InN, it was demonstrated that the 1LO peak position depends on the crystallographic orientation of the excited surface [6, 10, 12]. This dependence cannot be caused by scattering at the commonly assumed isotropic impurities. The change of the photon propagation direction by varying the excited surface can also be ruled out as an explanation as the wave vector of the photons is negligibly small compared with that of the involved phonons. We discuss this contradiction below in detail and present further additional experiments ruling out the influence of the light wave vector. To solve this problem, we introduce a model generalizing the elastic scattering process to be induced by any crystal defect that is localized in real space and can therefore break the $\vec{k}$-conservation. Starting from this, we show that, in addition to the established scattering mechanism at the impurities (i.e. point defects), elastic scattering at the surface (i.e. planar defects) can be observed and that these two processes can be distinguished experimentally. This can be used to gain access to surface properties as well as incorporated impurities of the sample, from which especially material scientists may greatly benefit.

Polarization resolved Raman spectra of InN in the literature show changes of the 1LO peak position with the polarization configuration [9, 13, 14], which have not been discussed so far. For the wide band gap materials, no polarization resolved UV Raman measurements have been published yet. In this paper, we demonstrate that the 1LO peak of ZnO and GaN exhibits similar

polarization behaviour as already observed for InN. We show that this phenomenon can also be understood in terms of the two distinct elastic scattering paths introduced above by postulating the polarization properties for them.

This paper is structured as follows: in section 2, we introduce our extended model and derive predictions for the Raman spectra. Subsequent to introducing our experimental conditions in section 3, we present our measurements on GaN, ZnO and CdS in section 4 to verify these predictions and discuss the results in section 5.

2. Theory

First, we recall the bases of Raman scattering in wurtztite crystals in general. In the second subsection, we explain the peculiarities in the case of resonant excitation above the band gap and elaborate the discrepancies between the experimental data and their interpretation in the literature. In section 2.3, we propose our model of 1LO Raman scattering due to the defects and then give a list of predictions resulting from it in section 2.4.

2.1. Non-resonant Raman scattering in wurtzite crystals

The wurtzite crystal structure belongs to the space group $P6_3mc$ in international and C_{6v}^4 in Schönflies notation. Its elementary unit cell consists of four atoms resulting in 12 phonon modes of which 9 are optically active. According to group theory, the optical phonon modes belong to the irreducible representation [15]

$$\Gamma_{\text{opt}} = A_1 + 2B_1 + E_1 + 2E_2 \tag{1}$$

at the Γ-point of the reciprocal space. The atomic motion is parallel to the c-axis for the A_1 and B_1 modes and perpendicular for the modes with E-symmetry. The A_1 and E_1 modes are polar and therefore split into transversal optical (TO) and longitudinal (LO) modes at the Γ-point. They are infrared and Raman active. The B_1 and E_2 modes are non-polar. While the E_2 modes are Raman active only, the B_1 modes are silent, i.e. neither Raman nor infrared active. Exemplarily, Raman spectra for GaN, ZnO and CdS excited below the band gap are shown in figure 2. These spectra were measured in two backscattering geometries, one with the light beam parallel $(z(xx)\bar{z})$ and one perpendicular $(x(y+z, y+z)\bar{x})$ to the crystal axis c, depicting the typical features of the wurtzite structure. Scattering geometries are given in Porto notation [15] $k_i(e_ie_s)k_s$ where k means the direction of the light wave vector within the sample and e the direction of the polarization while the indices denote the incident (i) and scattered (s) beam, respectively. The direction z is set parallel to the c-axis of the crystal, the notation $y+z$ denotes the direction (011).

The selection rules of the zone centre modes for selected scattering geometries as determined by the according Raman tensors [16] are summarized in table 1. They are only valid for deformation potential scattering which is the scattering mechanism for all nonpolar as well as polar TO modes while for the polar LO modes $\vec{q}$-dependent Fröhlich scattering can also occur. In the latter case, the selection rules of table 1 are no longer valid and 'forbidden' scattering can be observed. This might explain the observation of the weak E_1(LO) peak in figure 2 for GaN and CdS. As in the experiments typically focusing optics with high numerical apertures are used, the selection rules might also be softened by the non-ideal normal incidence causing the

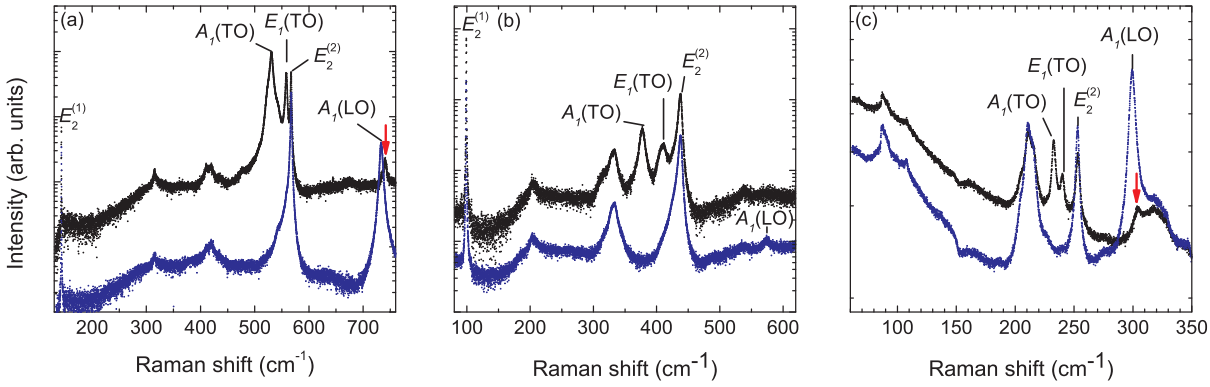

Figure 2. Representative Raman spectra of (a) GaN, (b) ZnO and (c) CdS excited on surfaces perpendicular ($z(xx)\bar{z}$, black) and parallel ($x(y+zy+z)\bar{x}$, blue) to the c-axis at $\lambda_{\text{exc}} = 532\,\text{nm}$ showing all expected Raman active modes of the wurtzite crystals. The peaks marked with an arrow are situated at the spectral position of the E_1(LO), which is however symmetrically forbidden in this scattering geometry (see the text). Peaks which are not labelled result from multi-phonon scattering processes.

Table 1. Selection rules for first-order Raman scattering by Γ-point phonons in the wurtzite structure.

Scattering geometry	Allowed phonon modes
$z(xx)\bar{z}$	A_1(LO), $E_2^{(2)}$
$z(xy)\bar{z}$	$E_2^{(2)}$
$x(yy)\bar{x}$	A_1(TO), $E_2^{(2)}$
$x(zz)\bar{x}$	A_1(TO)
$x(yz)\bar{x}$	E_1(TO)
$x(yz)y$	E_1(TO), E_1(LO)

appearance of the E_1(LO) peak. For ZnO, we do not observe E_1(LO) in backscattering geometry due to its small scattering cross section at $\lambda_{\text{exc}} = 532\,\text{nm}$.

In Raman scattering excited below the band gap, i.e. without the creation of real intermediate states, only three quasi-particles are involved: the incident and the scattered photon as well as the created (Stokes) or annihilated (anti-Stokes) phonon. For these, conservation of energy and momentum need to be fulfilled, i.e.

$$\hbar\omega_{\text{i}} = \hbar\omega_{\text{s}} \pm \hbar\omega_{\text{p}}, \tag{2}$$

$$\vec{k}_{\text{i}} = \vec{k}_{\text{s}} \pm \vec{q} \tag{3}$$

for the Stokes (+) and anti-Stokes (−) process, respectively. Here, ω_{i}, ω_{s} and ω_{p} are the frequencies of the incident and scattered light and of the phonon, respectively, and $\vec{q}$ is the phonon wave vector. In the case of backscattering $\vec{q} \approx 2\vec{k}_{\text{i}}$ is small enough, when compared with the extension of the Brillouin zone, that we can treat the phonons as Γ-point phonons. If the resulting $\vec{q}$ is neither parallel nor perpendicular to the c-axis, the strict distinction between

the A_1 and E_1 modes is no longer possible because the electrostatic forces causing the LO–TO-splitting dominate over the crystal anisotropy. This results in quasi-TO (qTO) and quasi-LO (qLO) modes situated energetically between A_1 and E_1. In the present paper, we deal only with LO phonons, the frequency of their respective qLO modes can be approximated by [16]

$$\omega_{\mathrm{qLO}} = \omega_{A_1(\mathrm{LO})} \cos^2 \beta + \omega_{E_1(\mathrm{LO})} \sin^2 \beta, \tag{4}$$

where β is the angle between the $\vec{q}$ and the c-axis.

2.2. Resonant Raman scattering

In the present paper, we investigate the case of the excitation energy above the band gap of the semiconductor. In this case, the Raman spectra of the wurtzite crystals typically exhibit a series of almost equidistantly spaced emission lines which are assigned to multiple scattering from LO phonons (nLO) [4, 17, 18]. An explanation for these high order processes is given in terms of the so-called cascade model [19] as depicted on the right hand side of figure 1. In a simplified excitonic picture, the incident photon creates a correlated electron–hole pair occupying a state in the exciton continuum. This can scatter by one LO phonon into a discrete exciton state which couples much stronger to the LO phonons via Fröhlich interaction than photons do. From such an intermediate discrete state the exciton can either scatter by another LO phonon into a lower energy (discrete) state or into a state near the Γ-point where it recombines by emitting the nLO Raman photon. Consequently, the spacing between the nLO lines is energetically slightly smaller than the Γ-point energy of the LO phonons.

For $n \geqslant 2$ the dominance of the cascade process described above is obvious because of the resonance with discrete exciton states [20, 21], while for $n = 1$ (1LO) the direct scattering processes near the Γ-point might be preferred. Martin [21] showed that the enhancement of the scattering intensity for excitation above the band gap for 1LO only occurs if at least one of the following prerequisites is fulfilled: a steep dispersion of the exciton resulting in wave vectors of the discrete exciton state at the excitation energy in the order of the light wave vector, parallel valence and conduction bands or a breakdown of momentum conservation. Because we treat the excitation well above the band gap and far below any other critical point, the first two possibilities can be ruled out. The origin of the remaining process able to enhance the scattering efficiency, i.e. the breakdown of momentum conservation, can be divided into two possibilities: the broadening of the light wave vector by absorption and elastic scattering induced e.g. by fields like the electric field due to a surface space charge region, or defects. In both cases, a redshift of the 1LO line with respect to the Γ-point phonon energy can be expected due to the contribution of phonons with larger wave vectors. We checked whether the broadening of the photon wave vector due to absorption could explain the magnitude of the experimentally observed redshift (cf section 4.1). For this purpose, we carried out a calculation based on the equation for the scattering cross section

$$\sigma = \sigma_0 \frac{\omega_\mathrm{s}}{\omega_\mathrm{i}} \int \mathrm{d}q_z f(q_z) \times |R(q, 0, \omega_\mathrm{i}, \omega_\mathrm{s})|^2 \times \delta(\omega_\mathrm{i} - \omega_\mathrm{s} - \omega_0(q)) \tag{5}$$

adopted from [21]. Hereby, R is the wave-vector-dependent Raman tensor element and $f(q_z)$ is a form factor representing the wave vector profile caused by the momentum conservation breaking mechanism, σ_0 is the Compton cross section and ω_i and ω_s the frequencies of the incident and scattered light, respectively. The result of this equation is a simulated spectrum which can be compared with the experimental data. Details of the calculation can be found in

appendix A. In short, the results show that the redshift which can be expected due to absorption is about one order of magnitude below the actually observed one. Therefore, the redshift cannot be explained by only taking the photon absorption into account. Davydov *et al* [10] previously showed experimentally that this redshift also depends on the energy of the exciting light. The Raman shift of the 1LO line thereby followed roughly that of the phonon energy at the wave vector of the discrete exciton states at the excitation energy. Conversely, the calculations show that the dominating range of the phonon wave vectors participating in the scattering process for the absorption case is mainly determined by the absorption coefficient and not by the exciton dispersion (cf figure A.1(b)). Thus, we conclude that only the scattering mechanism including elastic scattering by an inhomogeneity, i.e. defects of the perfect translational symmetric crystal, similar to the cascade process for larger n, can explain these experimental observations. This process is depicted on the left hand side of figure 1 and discussed in detail in the following.

2.3. Influence of the dimensionality of defects

We group defects according to the dimensionality of their spatial localization: three-dimensionally localized point defects, two-dimensionally localized line defects and one-dimensionally localized planar defects. The breakdown of $\vec{k}$-conservation, which is just a consequence of Heisenberg's uncertainty principle, only occurs in the directions of localization, e.g. only perpendicular to a planar defect. Consequently, only phonons from the respective directions of the Brillouin zone can cause the observation of 1LO emission. In the uniaxial wurtzite crystal structure the phonon energies differ according to whether their propagation is parallel or perpendicular to the crystal axis c, so their direction of propagation relative to the c-axis affects their spectral position.

In the following, we want to restrict ourselves to the contributions we actually observe experimentally, namely by the surface as a planar defect of the crystal and by point defects caused by impurities, and assume that excitation and detection are carried out on the same surface of the sample as is common for excitation above the band gap. We will call the spectral features, and the respective scattering mechanisms, related to the surface s1LO and those related to the impurities i1LO. According to the deliberations above, the spectral position of the s1LO feature is dependent on the crystallographic orientation of the surface within the excitation spot. For excitation on the c-plane, only scattering by phonons from the A_1(LO) phonon branch can lead to a 1LO emission while for excitation on the m- or a-plane, phonons from the E_1(LO) branch are required in the scattering process. We note that more precisely, also a difference between the spectra from the m- and a-planes is to be expected because of the slightly different phonon dispersions along the respective directions of the Brillouin zone. However, these differences are too small to observe any influence and we will therefore refrain from this distinction. These two excitation geometries represent the possible extrema regarding the energetic position of the 1LO line and will be distinguished by us as s1LO(A) and s1LO(E) according to the participating phonon mode branches. This process involving an elastic scattering step at the surface is substantially different from the concept of quasi-LO phonons observed for oblique Raman scattering geometries (see above) because of the large phonon wave vectors $|\vec{q}| \gg |\vec{k}_\mathrm{i} - \vec{k}_\mathrm{s}|$ involved, i.e. the light wave vectors do not determine the direction of the phonon propagation. In the scattering process involving elastic scattering by point defects, phonons from all directions of the Brillouin zone participate because of the

three-dimensional localization of the defect. As the s1LO(A) and s1LO(E) lines give the limits for the 1LO peak position, the i1LO line must be situated inbetween.

For comparative measurements between samples with larger and smaller amounts of incorporated impurities, the impurities need to be introduced intentionally. An obvious way to do this is doping. However, we would like to point out that dopants do not necessarily cause the i1LO contribution to the 1LO line except if the dopant creates an electric potential that is sufficiently strongly localized in real space or if it introduces other point defects for which this is true. The extension of a neutral shallow donor can be estimated from its Bohr radius which is between about 2 nm (ZnO, $m^* \approx 0.25 m_0$ [22]) and 10 nm (InN, $m^* \approx 0.06 m_0$ [23]) for the materials studied here. The resulting spread in $\vec{k}$-space is in case of ZnO near, but still below, the wave vector of the exciton branch at the excitation energy of 3.81 eV used in the experiments here. In contrast, nominally undoped crystals may contain a significant concentration of point defects enabling the observation of the i1LO scattering process.

The introduction of point defects by doping typically leads to an increase of the free charge carrier concentration which may also affect the energy of the polar phonon modes. The arising electron plasma couples with the LO phonons resulting in so-called coupled LO phonon-plasmon (LPP) modes which have two branches: LPP^+ and LPP^-. For the large phonon wave vectors that we are dealing with here, the LPP^+ mode becomes overdamped while the LPP^- mode shifts from the LO branch to the TO branch with increasing charge carrier concentration [24, 25]. Therefore, a decrease of the Raman shift would be expected with increasing doping. We actually observe this behaviour for higher-order LO lines, which is however out of the scope of this text. Consequently, the introduction of additional charge carriers might change the position of the observed i1LO line to lower energies. However, at least in our samples discussed here, the charge carrier concentration is low enough that it does not affect the qualitative shift between the i1LO line and the s1LO line.

2.4. Predictions of our model

From the considerations above, we derive several predictions for the exciton-mediated 1LO line in the Raman spectra of wurtzite semiconductors which we will prove experimentally in the following to verify our theory (the respective experimental section is given in parentheses):

- For crystals with a low concentration of point defects, the 1LO peak is dominated by the s1LO. Consequently, the position of the 1LO peak depends on the crystallographic orientation of the surface the excitation is carried out on (cf section 4.1).
- The position of the 1LO peak does not change with the angle of incidence on a particular surface and consequently does not show quasi-mode behaviour as described by (4) (cf section 4.1).
- A high concentration of point defects causes the additional i1LO contribution to the 1LO line, hence the integrated 1LO intensity increases (cf section 4.2).
- The spectral position of the i1LO line does not depend on the crystal orientation of the excited surface (cf section 4.2).

We further postulate properties for the polarization of the emitted light. It seems natural that, in the case of backscattering geometry, elastic scattering from the surface not only conserves the in-plane wave vector but also the polarization, which is in this case also in-plane. Therefore, we

Table 2. Properties of the 1LO lines due to s1LO and i1LO processes.

	s1LO	i1LO
Peak position dependent on excited surface	Yes	No
Appears in ideal crystal	Yes	No
Appears in parallel polarized configuration	Yes	Yes
Appears in cross polarized configuration	No	Yes

expect emission from the s1LO process to be parallel polarized with respect to the incident laser light. In contrast, we expect that the polarization is (partially) lost in the scattering process from a point defect and therefore we postulate the emission from the i1LO process to be (partially) depolarized. We thus predict for the expected spectra:

- the s1LO line is missing in the cross polarized spectrum, i.e. in the cross polarized spectrum only the i1LO line can be detected (cf section 4.3);
- the relative integrated intensity between the cross and parallel polarized 1LO peak is increased by the introduction of impurities (cf section 4.3).

The expected properties of the two contributions s1LO and i1LO are also summarized in table 2.

3. Experimental setup and samples

Excitation above the band gap was carried out by using the 325 nm line of an HeCd laser which emits highly linear polarized light. For comparison measurements with the excitation below the band gap a frequency doubled diode pumped solid state (DPSS) laser ($\lambda_{exc} = 532$ nm) was used. In both cases, the incident light was focused and the scattered light collected by a microscope objective (backscattering geometry) with a numerical aperture of 0.40 ($\lambda_{exc} = 325$ nm) and 0.42 ($\lambda_{exc} = 532$ nm), respectively. For measurements with tilted samples, a simple lens with a focal length of 20 mm and a smaller numerical aperture of about 0.26 was used instead of the objective. We checked for heating or high excitation effects by investigating the peak positions for different excitation powers and by the comparison between Stokes and anti-Stokes intensities of the $E_2^{(2)}$ line. For the measurements presented here, such effects can be excluded. All the measurements discussed here were carried out at room temperature. Measurements at low temperatures (down to $T \approx 10$ K) show principally identical results.

The scattered light was analysed for its linear polarization by means of a fixed Glan–Thompson prism together with a zero-order quartz $\lambda/2$-waveplate in front of the polarizer. The chromaticity of the waveplate can be neglected in the small spectral range examined here resulting in a deviation of the phase shift of less than 3% at 800 cm^{-1}.

Measurements at oblique incidence were carried out by simply tilting the sample, so still in backscattering geometry. We strictly used *s*-polarization, i.e. perpendicular to the plane of incidence, for excitation and detection in order to avoid a varying polarization component parallel to the *c*-axis (cf appendix B).

A Jobin Yvon U1000 Raman double spectrometer equipped with two 2400 lines mm^{-1} gratings and a liquid nitrogen cooled charge coupled device with 2048 × 512 square pixels with an edge length of 13.5 μm was used for spectrally resolved detection. The resolution of the

spectrometer is 6 pm which corresponds to an energetic resolution of 0.6 cm^{-1} in the spectral range near the HeCd laser line and 0.2 cm^{-1} near the DPSS laser line.

We investigated single crystals and films thick enough to exclude confinement effects in this study. Representatively for pure crystals, we used single crystals of ZnO (hydrothermally grown) from different commercial manufacturers (*c*-plane crystals from CrysTec, Eagle Picher, Tokyo Denpa and an *m*-plane crystal from CrysTec) yielding essentially identical results; GaN grown by hybrid vapour phase epitaxy (HVPE, by Freiberger Compound Materials); and CdS (from Crystal GmbH). Since there are no InN single crystals available, we used an MBE-grown thin film grown at Cornell University (sample Gs1768). The thickness of the InN layer is around 5.5 μm. It was grown on sapphire with subsequent AlN (130 nm) and GaN (175 nm) buffer layers and has a charge carrier concentration of around 5×10^{18} cm^{-1}.

For our comparative measurements between nominally doped and undoped crystals we studied only ZnO films because of the availability of suitable samples. In addition, ZnO has the benefit that its dopants usually cause the occurrence of defects breaking translational symmetry, which e.g. can be deduced from the observation of normally silent modes in the Raman spectrum excited below the band gap [26]. These ZnO films (thickness $d > 500$ nm) were grown by pulsed laser deposition (PLD). We used *a*-plane sapphire as substrate for *c*-oriented films and *r*-plane sapphire as substrate for *a*-oriented films [27]. A KrF excimer laser ($\lambda = 248$ nm, pulse energy 600 mJ) was used for ablation of the ceramic targets. The targets were ball-milled and subsequently sintered from ZnO powder with an addition of 1 at.% of Al_2O_3 for Al-doping and without addition for nominally undoped reference samples. The atmosphere in the PLD chamber was pure oxygen at a pressure of 0.02 mbar and the substrate holder was heated to 710 °C (*a*-sapphire) and 750 °C (*r*-sapphire), respectively. The films are of high quality and show typical ZnO properties; for more details cf [26, 28]. According to Hall measurements, the charge carrier concentration in the doped film is $n = 5 \times 10^{17}$ cm^{-3}.

4. Experimental results

4.1. Surface-related first-order longitudinal optical (1LO) line

Representative parallel polarized Raman spectra of undoped GaN, ZnO and CdS single crystals excited at $\lambda_{exc} = 325$ nm are shown in figure 3. The nonpolar $E_2^{(2)}$ mode and the TO modes (also the E_1(TO) mode not shown here) can be observed, but their intensity is much weaker compared with that typical for excitation below the band gap, which is caused by the small penetration depth of the UV light into the materials in the order of 100 nm. Their spectral positions and line broadenings are identical to measurements with excitation below the band gap and the selection rules are obeyed for these modes. (To be precise, the increased $\vec{k}$-vector of the UV light causes scattering by phonons with larger $\vec{q}$-vectors. However, even in the UV spectral region the light wavelength is too long compared with the unit cell dimensions to cause significant line shifts.)

The dominant feature in these spectra is lines in the region of the LO phonons. Their properties are different from the excitation below the band gap, but match our expectations for the s1LO line. The line positions are redshifted with respect to the respective zone centre phonons. The broadening is increased and the selection rules for the zone centre LO phonons are not valid for these lines. For GaN and ZnO the 1LO peak position depends on the orientation of the excited surface while for CdS only a very small difference is observed due to the small anisotropy splitting between the A_1(LO) and the E_1(LO) modes (see figure 3). As a

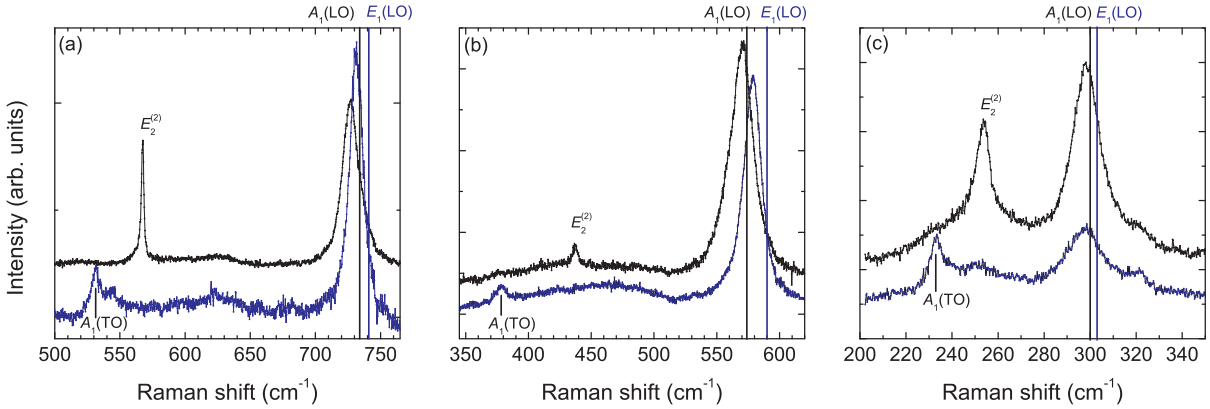

Figure 3. Raman spectra of nominally undoped (a) GaN, (b) ZnO and (c) CdS single crystals excited on surfaces perpendicular ($z(xx)\bar{z}$, black) and parallel ($x(zz)\bar{x}$, blue) to the c-axis at $\lambda_{exc} = 325$ nm. The spectra have been shifted vertically for clarity. In the GaN spectrum the photoluminescence background has been subtracted. The solid lines indicate the spectral position of the denoted zone centre LO phonons obtained with excitation below the band gap.

Table 3. Room temperature Raman shifts in cm^{-1} for the surface-related 1LO lines of wurtzite semiconductors excited at $\lambda_{exc} = 325$nm. The energies of the respective zone centre phonons are given in parentheses. All the cited literature values coincide with our own measurements; values without a reference given are based solely on our measurements. The given energies are the 1LO peak maxima in the $z(xx)\bar{z}$-configuration for the s1LO(A) line and in the $x(yy)\bar{x}$-configuration for the s1LO(E) line.

	ZnO	GaN	CdS
s1LO(A)	570[6] (574[29])	727 (734[30])	298.5 (300)
s1LO(E)	579[6] (590[29])	731 (741[30])	298 (303)

consequence, the results for CdS cannot be used to corroborate our predictions given above because a distinction between the different contributions from the spectral position is not possible. The experimental results for CdS are nevertheless in agreement with our model.

We summarized the 1LO peak positions for these three materials for $\lambda_{exc} = 325$ nm in table 3. Note that a dependence of the peak positions on the excitation energy is to be expected as was shown experimentally by Davydov *et al* [10] for InN, who observed that the s1LO peak position shifts towards lower energies with increasing excitation energy. Values for InN are not included in table 3, but can be found in that publication for a variety of excitation energies. Owing to the dependence of the peak position on the polarization relative to the c-axis (cf appendix B), we indicate the values for the $x(yy)\bar{x}$-configuration for our own measurements.

In order to further verify that the variation of the 1LO line position originates from the surface itself and not from the directions of the incident and scattered light wave vectors, we carried out oblique incidence measurements. For these, the samples were tilted by angles θ of 45° and 60°. This results, in the case of ZnO, in angles β of the internal light wave propagation

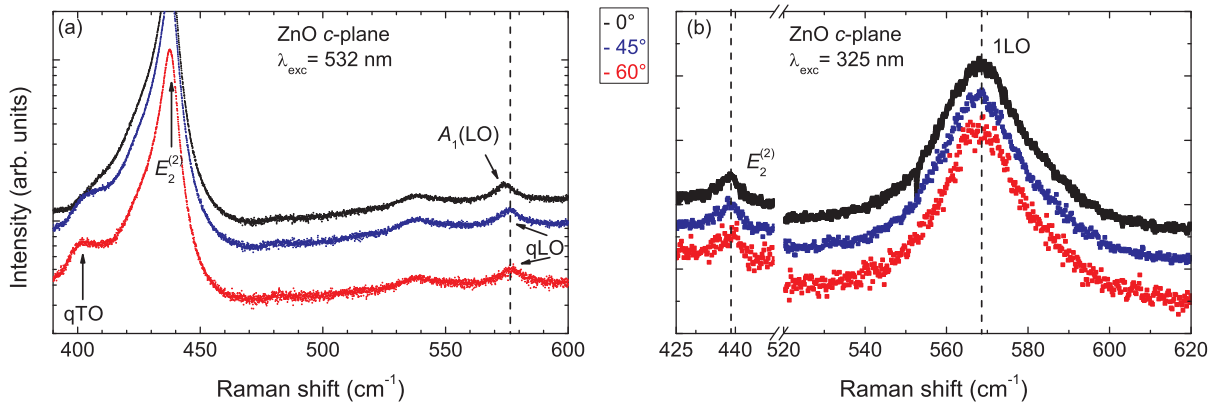

Figure 4. Raman spectra with varying sample tilt of ZnO in $k(xx)\bar{k}$ configuration with the external angle between $\vec{k}$ and the c-axis from 0 to 60° (from upper to lower curve) given in the legend, (a) $\lambda_{exc} = 532\,nm$ and (b) $\lambda_{exc} = 325\,nm$. The dashed line indicates the peak position at $\theta = 45°$. Note the logarithmic intensity scale for (a) and the linear intensity scale for (b). The spectra have been shifted vertically for clarity.

relative to the c-axis of about 21° and 26° (coincidentally the refractive index is $n \approx 2$ for both 325 and 532 nm as determined by spectroscopic ellipsometry), respectively. We will treat the c-plane as an example and initially assume that the 1LO mode shows quasi-mode behaviour while changing the angle of incidence, i.e. we describe its angular dependence by (4). According to this equation and by using $\omega_{s1LO(A)} = 570\,cm^{-1}$ and $\omega_{s1LO(E)} = 579\,cm^{-1}$ (see table 3), we would expect a blueshift of 1 and 1.5 cm^{-1} for θ of 45° and 60°, respectively. This is significant regarding the spectrometer's resolution. We used the spectrally fixed $E_2^{(2)}$ line (ZnO, GaN) and an argon gas low pressure lamp (InN) to ensure relative accuracy of the Raman shifts of below 0.1 cm^{-1}. While for $\lambda_{exc} = 532\,nm$ the expected blueshift is obvious at both angles, no shift can be observed for $\lambda_{exc} = 325\,nm$ even at $\theta = 60°$ (see figure 4). We observed the same behaviour for c-GaN (see figure 5) and for ZnO excited on the m-plane (see figure 6(a)). Also, the spectra of the c-InN film (see figure 6(b)) do not show a shift of the 1LO line as far as this can be judged despite the low intensity of the spectra. No comparative spectra are shown for ZnO because the E_1(LO) line is forbidden in backscattering geometry (cf figure 2(b)) and for InN because we are not able to excite it below its band gap. As a consequence of these results, we verified that the dependence of the 1LO line position on the excited surface is not a simple consequence of quasi-LO mode behaviour and the direction of the photon wave vectors has no decisive influence on the direction of the wave vectors of the phonons involved in the scattering process.

4.2. Impurity-related 1LO line

In order to investigate the influence of defects on the 1LO line, we compared the parallel polarized Raman spectra of nominally doped and undoped samples in figure 7. According to our predictions (see table 2), we expect both contributions s1LO and i1LO to be observable in this configuration. We observe increased intensity as well as increased broadening of the 1LO line for the doped samples for both crystallographic orientations of the excited surface. This is in agreement with the concept of the i1LO as an additional contribution in the scattering

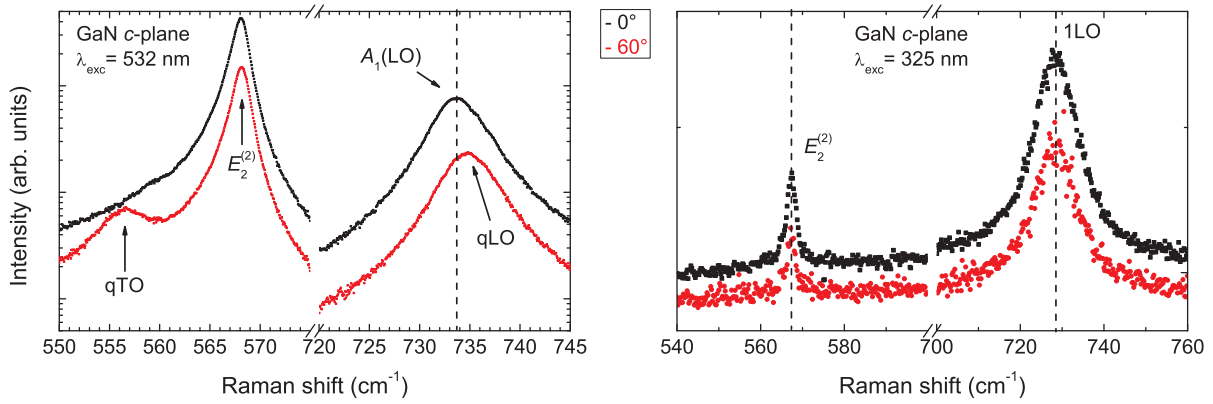

Figure 5. Raman spectra of varying sample tilt of a c-GaN single crystal excited at (a) $\lambda_{exc} = 532\,nm$ and (b) $\lambda_{exc} = 325\,nm$ in $k(xx)\bar{k}$ configuration with the external angle between $\vec{k}$ and the c-axes of 0° and 60°, respectively. The dashed lines indicate the respective peak positions at $\theta = 0°$. Note the logarithmic intensity scale for (a) and the linear intensity scale for (b). The spectra have been shifted vertically for clarity.

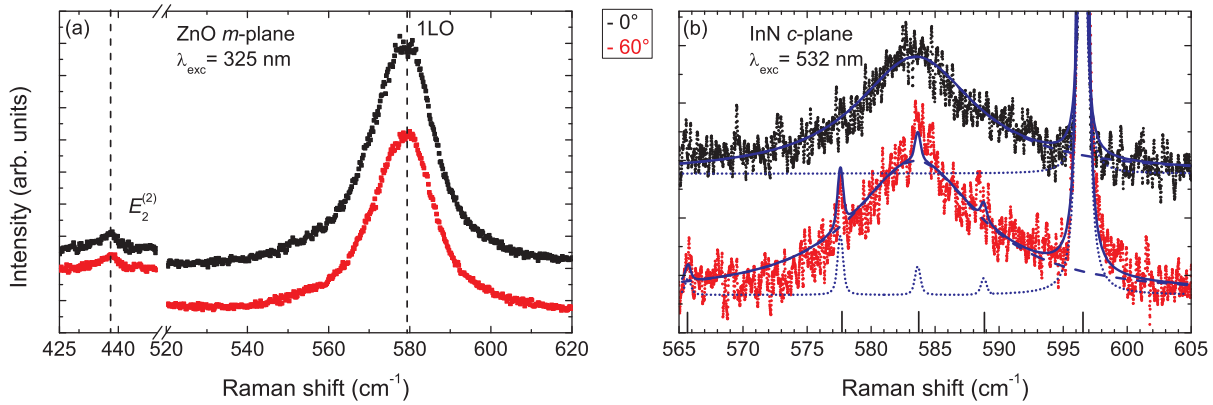

Figure 6. Raman spectra of varying sample tilt of (a) an m-ZnO single crystal excited at $\lambda_{exc} = 325\,nm$ and (b) a c-InN thin film excited at $\lambda_{exc} = 532\,nm$ in $k(xx)\bar{k}$ configuration with the external angle between $\vec{k}$ and the (a) $[1\bar{1}00]$-axis and (b) c-axes of 0° and 60°, respectively. The spectra have been shifted vertically for clarity. The dashed vertical lines in (a) indicate the respective peak positions at $\theta = 0°$. In (b), the 1LO lines are fitted with Lorentzian functions with identical spectral positions shown as dashed curves. Line fits of the argon lamp spectrum are shown as dotted lines, the solid line represents the sum of these fitted curves. Note that the relative intensity of the argon lines is stronger by a factor of around 4 in the spectrum measured at 60°. The spectral positions of the argon lamp lines are marked by black bars at the bottom of the graph.

process at a slightly different spectral position (cf section 2.3). The intensity maximum of the undoped samples is at the spectral position of the s1LO(A) for excitation on the c-plane and at the spectral position of the s1LO(E) for excitation on the a-plane, respectively. We observe that for the doped samples, the 1LO line is shifted to a position between these two extrema,

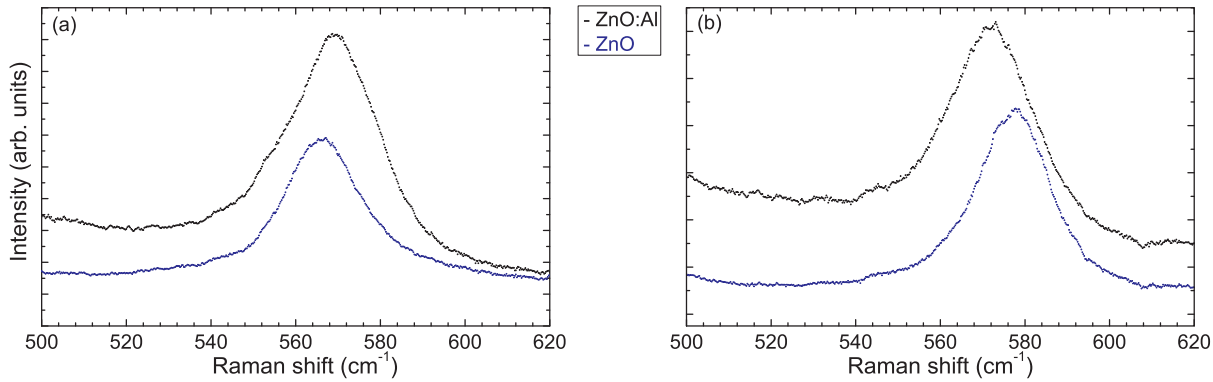

Figure 7. Parallel polarized Raman spectra of the 1LO lines of aluminium doped (1 at.% Al in the PLD target, black) and nominally undoped ZnO thin films (blue) excited on (a) the *c*-plane and (b) the *a*-plane at $\lambda_{exc} = 325$ nm.

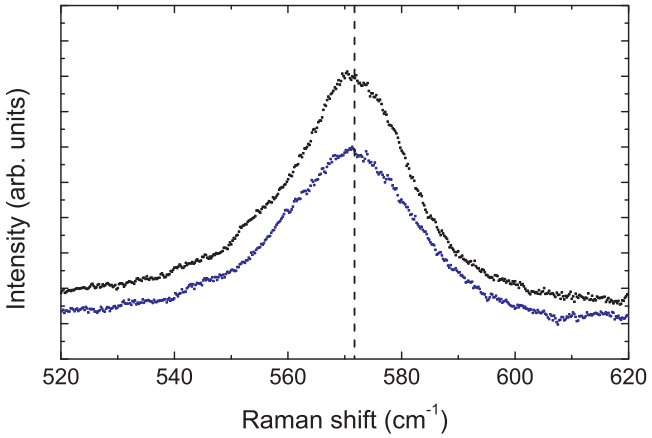

Figure 8. Raman spectra in cross polarized configuration for *c*- $(z(xy)\bar{z}$, black) and *a*-plane $(x(yz)\bar{x}$, blue) ZnO:Al thin films excited at $\lambda_{exc} = 325$ nm.

i.e. into the direction where we expect the i1LO line. The small deviation between the peak positions of the two doped samples results from the still present s1LO contribution. Actually, in the cross polarized spectra shown in figure 8, where the s1LO contribution is expected to vanish according to table 2, the 1LO peak positions are identical for both doped samples.

4.3. Polarization dependence

We compared the parallel and cross polarized spectra of nominally undoped single crystals to verify our postulated polarization properties. The polarization dependence of the 1LO line for excitation on the *c*-plane of GaN and ZnO is depicted in figure 9. For both the materials, the peak in the cross polarized spectrum is very weak and shifted to higher energies compared with the parallel polarized spectrum. This agrees with our expectation that only the i1LO line, which is supposed to be weak in pure single crystals, can be observed in the cross polarized configuration.

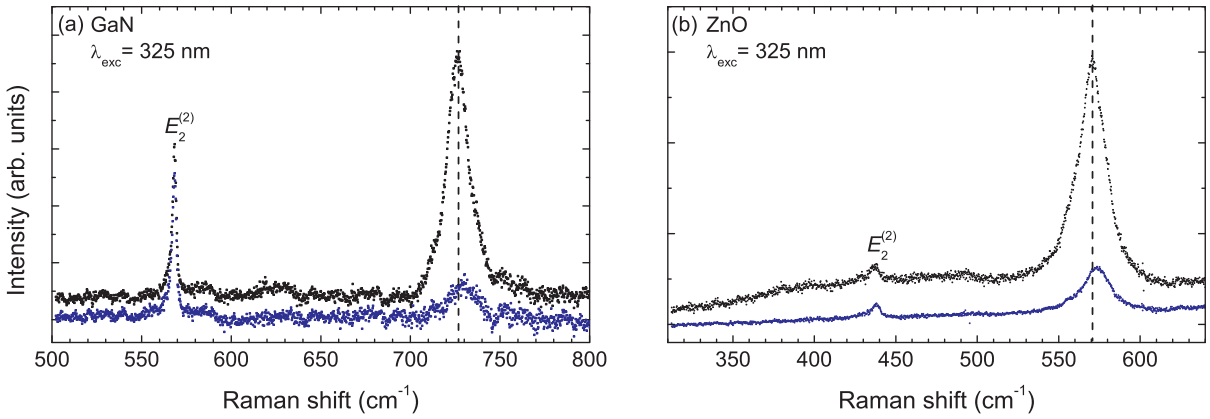

Figure 9. Raman spectra in parallel polarized $(z(xx)\bar{z}$, black) and cross polarized $(z(xy)\bar{z}$, blue) configuration for c-plane (a) GaN and (b) ZnO single crystals excited at $\lambda_{exc} = 325$ nm. In the GaN spectra, the photoluminescence background has been subtracted and the spectra have been shifted vertically for clarity. The dashed lines indicate the 1LO line positions in the parallel polarized spectra.

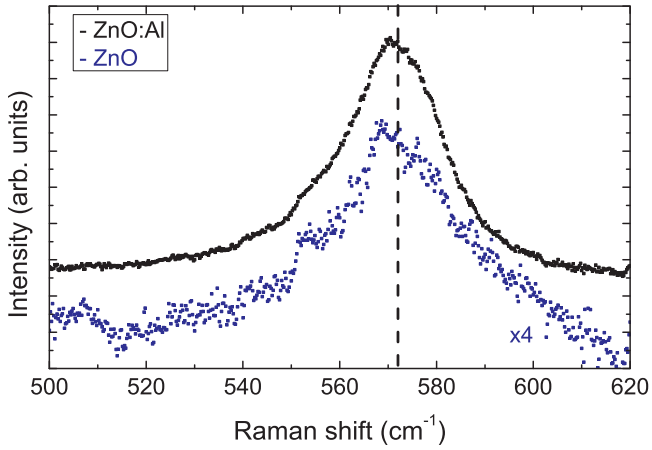

Figure 10. Cross polarized Raman spectra of the 1LO lines of aluminium doped (1 at.% Al in the PLD target, black) and nominally undoped ZnO films (blue) excited on the c-plane at $\lambda_{exc} = 325$ nm. The films are the same as in figure 7(a), the intensity range is lower by a factor of 4 than for that of the parallel polarized spectrum. For the spectrum of the undoped film, the photoluminescence background has been subtracted. The dashed line indicates the 1LO line positions for the doped crystal.

To further confirm that only the i1LO line is observed in the cross polarized spectra, we compared the cross polarized spectra of nominally doped and undoped ZnO thin films as shown in figure 10. While the parallel polarized 1LO peak is shifted in the doped sample as discussed above (cf figure 7(a)), the spectral position and also the line shape of the cross polarized one remain unchanged. This is again consistent with our model expecting only the i1LO contribution in the cross polarized spectra which results in the same Raman shift for both the samples. In addition, the intensity ratio between the doped and the undoped samples is larger in the cross

polarized configuration than in the parallel polarized one. In the latter case, the s1LO process equally contributes to the spectra of both samples and consequently reduces the intensity ratio.

5. Discussion

5.1. Surface-related 1LO line

We have shown in section 4.1 that the 1LO peak position in ideal wurtzites is exclusively determined by the crystallographic orientation of the excited surface itself and not by the scattering geometry. The peak position of the 1LO line stays constant for all tilting angles (figure 4) proving its independence of the wave vectors of the incident and scattered photons.

The dependence of the 1LO line on the crystal orientation of the excited surface has also been reported before for ZnO [6, 12] as well as for InN [10]. Bergmann *et al* [12] and Alarcón-Lladó *et al* [6], the latter also presenting Raman spectra for excitation on two additional crystal cuts not investigated here, ascribed this face dependence to the quasi-LO modes. This is in disagreement with both the magnitude of the redshift of the 1LO line with respect to the Γ-point phonon energy and the oblique incidence measurements we are presenting here. Davydov *et al* [10] explained their observations based on the elastic scattering by the impurities also considered here for the i1LO process, but did not give a reason for the face dependence of the peak position. In none of these publications is a motivation given on how the small photon wave vector shall determine the direction of the large phonon wave vector causing the redshift of the 1LO line. In contrast, our model including a process breaking the translational symmetry which involves the surface can conclusively explain all these experimental observations.

5.2. Impurity-related 1LO line

The elastic scattering by the impurities can also be observed in the Raman spectra of wurtzites excited above the band gap. Obviously, its influence increases with defect concentration. Such an additional contribution of the i1LO process was observed for Mg-doped InN [10, 31]. In particular, the doping series reported in [31] for InN:Mg nicely shows how the i1LO peak increases in intensity until it dominates the s1LO peak. This observation was attributed by the authors to increasing activation of the forbidden E_1(LO) phonon by the impurities. This description is to some extent comparable with our model for the i1LO line, excluding the fact that we expect contributions from all directions of the Brillouin zone. However, our model has the advantage that it does not suggest the occurrence of an impurity induced A_1(LO) line for *a*-InN:Mg, which was indeed not observed experimentally in these papers.

Pastor *et al* [32] also observed an increase in the intensity of the 1LO line with increasing Be-implantation in GaN as we expect from our model. Owing to the high charge carrier concentrations in their samples, the 1LO lines are shifted to lower energies for higher implementation doses as described in section 2. This superimposes the blueshift which we would expect due to the dominance of the i1LO line. Therefore, it is not possible to compare the peak positions observed by them with our values from table 3.

5.3. Polarization dependence

We have further shown that our postulated polarization properties for the two different contributions s1LO and i1LO are consistent with our experimental data. As we mentioned in the introduction, polarization resolved Raman spectra excited above the band gap of ZnO and GaN for comparison are missing in the literature. For InN, also a shift of the 1LO line between the parallel and the cross polarized peak similar to our findings can be seen in previously published spectra [9, 13, 14], but this shift was not discussed there. We conclude that the importance of the polarization dependence of the 1LO line might have been underestimated until now, especially for UV excitation of wide band gap materials, and it should be taken greater care of in the future.

6. Summary

We have introduced an extended model for the description of the exciton mediated 1LO Raman scattering in wurtzite type semiconductors. It considers two different elastic scattering mechanisms breaking $\vec{k}$-conservation: one related to the surface, which we call s1LO, and one related to the point defects, which we call i1LO. The decisive influence of the crystallographic orientation of the surface on the 1LO peak position is evident as proven by our oblique incidence measurements for ZnO and GaN. The wide analogues in the properties of the 1LO line between all wurtzites under investigation (GaN, ZnO, CdS and InN) strongly suggest this to be a universal feature of at least the wurtzite crystals. The observed dependence of the 1LO peak position on the crystallographic orientation of the excited surface vanishes if only elastic scattering by point-like defects is observed, either because of a high defect concentration or of the polarization configuration. We have postulated that the s1LO contribution is only observed in the parallel polarized scattering configuration while the i1LO contribution can also be observed for cross polarization. These postulated polarization properties have been validated by several experimental findings.

Acknowledgments

This work has been partially funded by the Deutsche Forschungsgemeinschaft in the framework of SFB 762 'Functionality of Oxide Interfaces'. CK was funded by the European Union and the Free State of Saxony. We wish to thank Gunnar Leibiger (Freiberger Compound Materials) for supplying the GaN samples, William Schaff (Cornell University) for supplying the InN sample, Holger Hochmuth for PLD growth of the ZnO films and Chris Sturm for valuable discussions.

Appendix A. Calculation of theoretical spectra

We modified (5) in two points. We substituted the delta-distribution in the equation by a convolution with LO phonons with Lorentzian broadening by using the known linewidth of the Γ-point phonons as constant broadening. The phonon dispersion was taken from the inelastic neutron scattering data for ZnO [33] and from the theoretical calculations based on a modified valence-force model [34]. It is in the nature of these methods that their accuracy is worse than that of the Raman measurements. Consequently, the accuracy of our calculations based on these data is in turn limited.

Table A.1. Parameters for the calculation of the Raman tensor: lattice parameters a_0 and c_0, band gap E_g, effective electron and hole masses m_e^* and m_h^*, exciton lifetime broadening Γ_{ex}, exciton binding energy E_{ex}, exciton Bohr radius $a_{B,ex}$, spin–orbit splitting Δ_{SO}, refractive index n_r, low and high frequency dielectric constants ϵ_0 and ϵ_∞, absorption coefficient α at $\lambda_{exc} = 325$ nm and phonon mode broadening $\Gamma(A_1(LO))$ and $\Gamma(E_1(LO))$.

Parameter	ZnO	GaN
a_0	3.25 Å[a]	3.19 Å[b]
c_0	5.105 Å[a]	5.19 Å[b]
E_g	3.37 eV[c]	3.39 eV[d]
m_e^*	0.28 m_e [e]	0.2 m_e [f]
m_h^*	2.4 m_e [e]	2.0 m_e [f]
Γ_{ex}	46 meV[g]	40 meV[g]
E_{ex}	63 meV[h]	21 meV[i]
$a_{B,ex}$	1.5 nm[j]	2.8 nm[j]
Δ_{SO}	−12 meV[k]	−8 meV[l]
n_r	2.0[m]	2.6[n]
ϵ_0	8.2[m]	10.9[n]
ϵ_∞	3.6[m]	5.35[n]
α	1.6×10^5 cm^{-1} [o]	1.2×10^5 cm^{-1} [p]
$\Gamma(A_1(LO))$	9.7 cm^{-1} [q]	5.7 cm^{-1} [r]
$\Gamma(E_1(LO))$	11.7 cm^{-1} [q]	6.7 cm^{-1} [r]

[a] Karzel *et al* [36].
[b] Lagerstedt and Monemar [37].
[c] Klingshirn [38].
[d] Maruska and Tietjen [39].
[e] Jang and Chichibu [22].
[f] Kim *et al* [40].
[g] Broadening of near band edge luminescence.
[h] Mang *et al* [41].
[i] Shan *et al* [42].
[j] Calculated.
[k] Lambrecht *et al* [43].
[l] Bougrov *et al* [44].
[m] Ellipsometry measurements.
[n] Benedict *et al* [45].
[o] Muth *et al* [46].
[p] Muth *et al* [47].
[q] Cuscó *et al* [29].
[r] Raman measurements at $\lambda_{exc} = 532$ nm.

The second modification affects the Raman tensor for which we used the more complex Fröhlich term taken from [35]. We restricted ourselves to a single exciton branch with parabolic dispersion. We did not use any free parameter but only values taken from the literature or from our own measurements. These are summarized in table A.1. The electronic system was treated as being isotopic, but the uniaxiality was taken into account for the phonon mode energies.

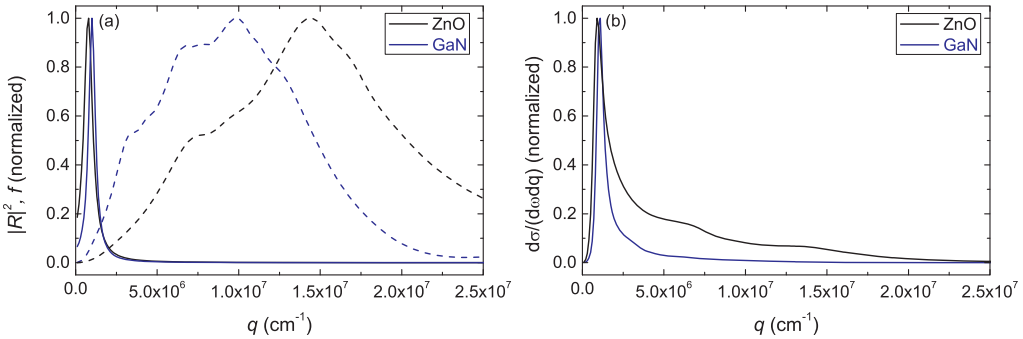

Figure A.1. (a) Squared absolute Raman tensor element $|R|^2$ (dashed line) and form factor f (solid line) for the case of photon absorption and (b) differential scattering cross section for photon absorption, mainly resembling the form factor f and only showing a small influence of $|R|^2$. Calculated for $\lambda_{\mathrm{exc}} = 325$ nm.

We compared two cases: breakdown of the wave vector conservation by photon absorption as described by the function

$$f(q_z) = \frac{1}{\pi} \frac{2\alpha}{(2k_0 - q_z)^2 + (2\alpha)^2} \tag{A.1}$$

adopted from [21] and elastic scattering of the exciton at the surface, which we ascribe to a constant function $f(q_z)$. Here, α is the absorption coefficient of the material and k_0 the wave vector of the propagating excitation light.

The wave vector dependences of R and f are shown in figure A.1(a). The maximum of the Raman tensor element R appears to be around $1.0 \times 10^7\,\mathrm{cm}^{-1}$ for GaN and around $1.4 \times 10^7\,\mathrm{cm}^{-1}$ for ZnO, which is, as expected, in the region of the wave vector of the discrete exciton branch at the excitation energy. The maximum of the form factor f is below $1.0 \times 10^6\,\mathrm{cm}^{-1}$ for both materials and decreasing rapidly with increasing wave vector. The differential scattering cross section $\mathrm{d}\sigma/(\mathrm{d}\omega\,\mathrm{d}q)$, being the product of $|R|^2$ and f, shows also a maximum around $1.0 \times 10^6\,\mathrm{cm}^{-1}$ and only small contributions of phonons with larger wave vectors (see figure A.1(b)). Obviously, the exciton dispersion influences the differential scattering cross section only slightly. The differential scattering cross section for the case of elastic scattering is identical to the curves for the squared Raman tensor element in figure A.1(a), because we assumed a flat function f.

The convolution of the differential scattering cross section with Lorentzians with a centre energy following the phonon dispersion of the two materials delivers the calculated spectra, shown for ZnO in figure A.2. Already from these spectra it is obvious that the calculated peak for the elastic scattering at the surface is closer to the experimental data than the result for the photon absorption case. Table A.2 shows this even more clearly. The redshift which can be expected due to the absorption of the incident light is by far insufficient to explain the experimentally observed peak maxima, while for elastic scattering a good match is observed. Only GaN excited on a surface perpendicular to the c-axis might be seen as an exception. Here, the very small calculated shifts result from the theoretical phonon dispersion which is mainly flat around the Γ-point [34]. For ZnO, inelastic neutron scattering revealed a much steeper phonon dispersion in this region than theoretically calculated, so this might also be the case for GaN, possibly explaining the too small redshift determined by us.

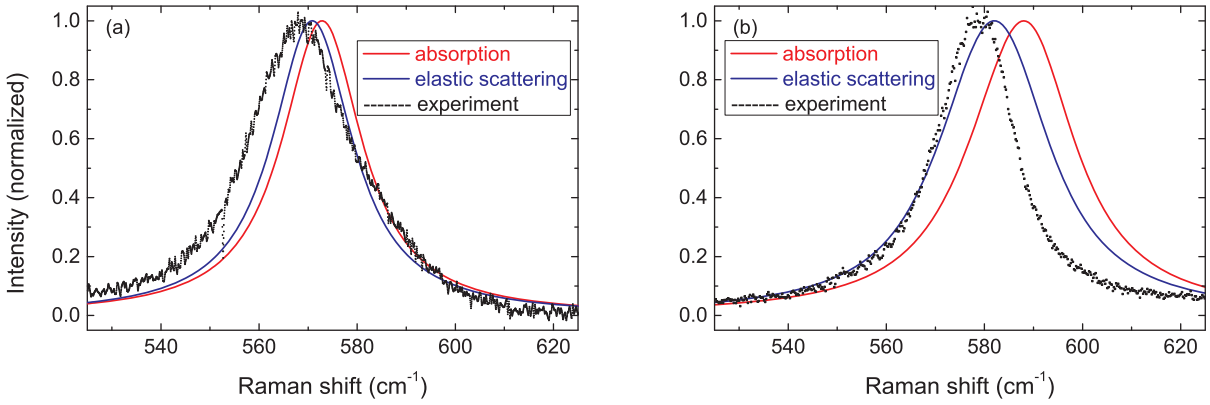

Figure A.2. Theoretically calculated spectra (solid lines) for ZnO excited on a surface (a) perpendicular and (b) parallel to the surface, and respective experimental data (scatter plot), all for $\lambda_{exc} = 325$ nm.

Table A.2. Calculated and experimental peak positions and redshifts relative to the zone centre phonon energies of the 1LO line at $\lambda_{exc} = 325$ nm.

	Theory				Experiment	
	Photon absorption		Elastic scattering			
	ZnO	GaN	ZnO	GaN	ZnO	GaN
Peak position $k \| c$	572.8	733.5	570.8	730.0	570	727
Redshift to A_1(LO)	1.2	0.5	3.2	4.0	4	7
Peak position $k \perp c$	588.1	740.8	582.1	739.5	579	731
Redshift to E_1(LO)	2.9	0.2	7.9	1.5	12	10

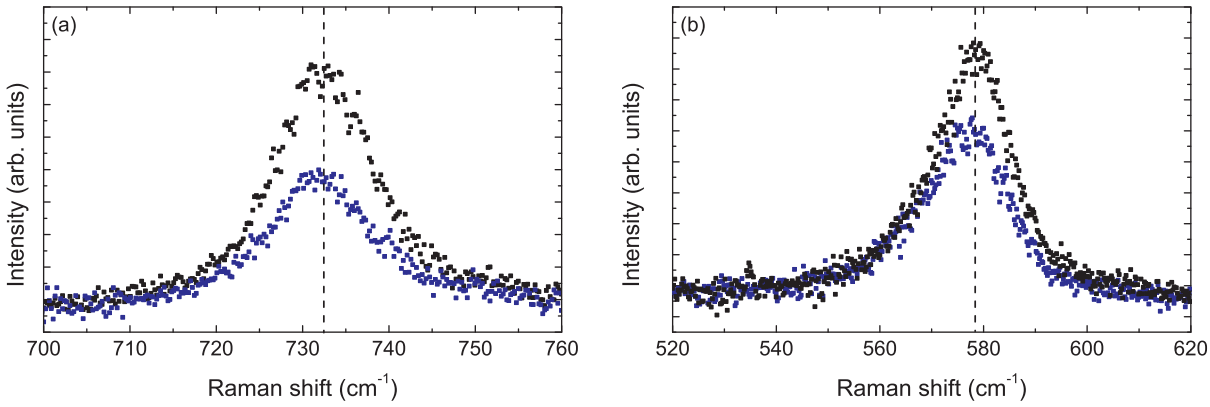

Figure B.1. Raman spectra of GaN (a) and ZnO (b) in $x(zz)\bar{x}$- (black) and $x(yy)\bar{x}$-configuration (blue) excited at $\lambda_{exc} = 325$ nm. The dashed line indicates the peak maximum of the $x(zz)\bar{x}$-spectra.

Appendix B. Polarization relative to the *c*-axis

An additional effect can be observed for parallel polarized measurements excited on a surface parallel to the c-axis: the dependence of the 1LO peak on the direction of the light polarization relative to the c-axis. This is depicted in figure B.1. For ZnO (b), the Raman shift is larger by approximately $1.5\,\mathrm{cm}^{-1}$ and the peak intensity is increased for the $x(zz)\bar{x}$- compared with the $x(yy)\bar{x}$-configuration. The shifting of the 1LO peak is less pronounced for GaN (a) showing a blueshift in the $x(zz)\bar{x}$-configuration of $0.4\,\mathrm{cm}^{-1}$ with respect to the $x(yy)\bar{x}$-configuration. However, a similar change of the peak intensity as for ZnO is obvious also for GaN. These observations would not be expected in the simple picture with only one exciton-like branch as depicted in figure 1 which does not include a dependence on light polarization. In wurtzite crystals however, light polarized perpendicular to the c-axis couples mainly to the two exciton branches A and B while light polarized parallel to the c-axis couples mainly with the C-excitons [48]. The differences in exciton dispersions possibly lead to different volumes in $\vec{q}$-space of phonons participating in the scattering process and therefore to different peak positions. A close inspection of the previously published Raman spectra of InN [13] also shows this very small deviation which was not discussed there.

References

[1] Gogolin A and Rashba E 1976 *Solid State Commun.* **19** 1177–9
[2] Trallero-Giner C, Cantarero A, Cardona M and Mora M 1992 *Phys. Rev.* B **45** 6601–13
[3] Menéndez J and Cardona M 1985 *Phys. Rev.* B **31** 3696–704
[4] Scott J F 1970 *Phys. Rev.* B **2** 1209–11
[5] Alexson D, Bergman L, Nemanich R J, Dutta M, Stroscio M A, Parker C A, Bedair S M, El-Masry N A and Adar F 2001 *J. Appl. Phys.* **89** 798–800
[6] Alarcón-Lladó E, Ibáñez J, Cuscó R, Artús L, Prades J D, Estradé S and Morante J R 2011 *J. Raman Spectrosc.* **42** 153–9
[7] Ng H T, Chen B, Li J, Han J, Meyyappan M, Wu J, Li S X and Haller E E 2003 *Appl. Phys. Lett.* **82** 2023–5
[8] Alim K A, Fonoberov V A and Balandin A A 2005 *Appl. Phys. Lett.* **86** 053103
[9] Kasic A, Schubert M, Saito Y, Nanishi Y and Wagner G 2002 *Phys. Rev.* B **65** 115206
[10] Davydov V Y, Klochikhin A A, Smirnov A N, Strashkova I Y, Krylov A S, Lu H, Schaff W J, Lee H M, Hong Y L and Gwo S 2009 *Phys. Rev.* B **80** 081204
[11] Thakur J S, Haddad D, Naik V M, Naik R, Auner G W, Lu H and Schaff W J 2005 *Phys. Rev.* B **71** 115203
[12] Bergman L, Chen X B, Huso J, Morrison J L and Hoeck H 2005 *J. Appl. Phys.* **98** 093507
[13] Davydov V Y, Emtsev V V, Goncharuk I N, Smirnov A N, Petrikov V D, Mamutin V V, Vekshin V A, Ivanov S V, Smirnov M B and Inushimakk T 1999 *Appl. Phys. Lett.* **75** 3297–9
[14] Kaczmarczyk G *et al* 2000 *Appl. Phys. Lett.* **76** 2122–4
[15] Damen T C, Porto S P S and Tell B 1966 *Phys. Rev.* **142** 570–4
[16] Loudon R 1964 *Adv. Phys.* **13** 423–82
[17] Leite R C C, Scott J F and Damen T C 1969 *Phys. Rev. Lett.* **22** 780–2
[18] Klein M V and Porto S P S 1969 *Phys. Rev. Lett.* **22** 782–4
[19] Yu P Y and Cardona M 1996 *Fundamentals of Semiconductors: Physics and Materials Properties* (Berlin: Springer) (http://springerlink.com/content/p61h8n/?p=118fa8b314f043adbc16f55562b5e88a&pi=0)
[20] Martin R M and Varma C M 1971 *Phys. Rev. Lett.* **26** 1241–4
[21] Martin R M 1974 *Phys. Rev.* B **10** 2620–31
[22] Jang S H and Chichibu S F 2012 *J. Appl. Phys.* **112** 073503

[23] Millot M, Ubrig N, Poumirol J M, Gherasoiu I, Walukiewicz W, George S, Portugall O, Léotin J, Goiran M and Broto J M 2011 *Phys. Rev.* B **83** 125204
[24] Abstreiter G, Trommer R, Cardona M and Pinczuk A 1979 *Solid State Commun.* **30** 703–7
[25] Olego D and Cardona M 1981 *Phys. Rev.* B **24** 7217–32
[26] Bundesmann C, Ashkenov N, Schubert M, Spemann D, Butz T, Kaidashev E M, Lorenz M and Grundmann M 2003 *Appl. Phys. Lett.* **83** 1974–6
[27] Bundesmann C, Ashkenov N, Schubert M, Rahm A, Wenckstern H, Kaidashev E, Lorenz M and Grundmann M 2004 *Thin Solid Films* **455–456** 161–6
[28] Brandt M *et al* 2010 *Phys. Rev.* B **81** 073306
[29] Cuscó R, Alarcón-Lladó E, Ibáñez J, Artús L, Jiménez J, Wang B and Callahan M J 2007 *Phys. Rev.* B **75** 165202
[30] Davydov V Y, Kitaev Y E, Goncharuk I N, Smirnov A N, Graul J, Semchinova O, Uffmann D, Smirnov M B, Mirgorodsky A P and Evarestov R A 1998 *Phys. Rev.* B **58** 12899–907
[31] Davydov V Y, Klochikhin A A, Smirnov A N, Strashkova I Y, Krylov A S, Hai L, Schaff W J, Lee H M, Hong Y L and Gwo S 2010 *Semiconductors* **44** 161–70
[32] Pastor D, Ibañez J, Cuscó R, Artús L, González-Díaz G and Calleja E 2007 *Semicond. Sci. Technol.* **22** 70
[33] Serrano J, Manjón F J, Romero A H, Ivanov A, Cardona M, Lauck R, Bosak A and Krisch M 2010 *Phys. Rev.* B **81** 174304
[34] Siegle H, Kaczmarczyk G, Filippidis L, Litvinchuk A P, Hoffmann A and Thomsen C 1997 *Phys. Rev.* B **55** 7000–4
[35] Trallero-Giner C, Cantarero A and Cardona M 1989 *Phys. Rev.* B **40** 4030–6
[36] Karzel H *et al* 1996 *Phys. Rev.* B **53** 11425–38
[37] Lagerstedt O and Monemar B 1979 *Phys. Rev.* B **19** 3064–70
[38] Klingshirn C 1975 *Phys. Status Solidi* b **71** 547–56
[39] Maruska H P and Tietjen J J 1969 *Appl. Phys. Lett.* **15** 327–9
[40] Kim K, Lambrecht W R L, Segall B and van Schilfgaarde M 1997 *Phys. Rev.* B **56** 7363–75
[41] Mang A, Reimann K and Rübenacke S 1995 *Solid State Commun.* **94** 251–4
[42] Shan W, Little B D, Fischer A J, Song J J, Goldenberg B, Perry W G, Bremser M D and Davis R F 1996 *Phys. Rev.* B **54** 16369–72
[43] Lambrecht W R L, Rodina A V, Limpijumnong S, Segall B and Meyer B K 2002 *Phys. Rev.* B **65** 075207
[44] Bougrov V, Levinshtein S, Rumyantsev S and Zubrilov A 2001 *Properties of Advanced Semiconductor Materials—GaN, AIN, InN, BN, SiC, SiGe* 1st edn (New York: Wiley) chapter 1 pp 1–30
[45] Benedict L, Wethkamp T, Wilmers K, Cobet C, Esser N, Shirley E, Richter W and Cardona M 1999 *Solid State Commun.* **112** 129–33
[46] Muth J F, Kolbas R M, Sharma A K, Oktyabrsky S and Narayan J 1999 *J. Appl. Phys.* **85** 7884–7
[47] Muth J F, Lee J H, Shmagin I K, Kolbas R M H C, Casey J, Keller B P, Mishra U K and DenBaars S P 1997 *Appl. Phys. Lett.* **71** 2572–4
[48] Liang W Y and Yoffe A D 1968 *Phys. Rev. Lett.* **20** 59–62